scientific reports

Check for updates

OPEN

Flow investigation of the stagnation point flow of micropolar viscoelastic fluid with modified Fourier and Fick's law

Muhammad Naveed Khan[1], Aamir Abbas Khan[2], Zhentao Wang[1]✉, Haifaa F. Alrihieli[3], Sayed M. Eldin[4], F. M. Aldosari[5] & Ibrahim E. Elseesy[6]

Non-Newtonian fluids are extensively employed in many different industries, such as the processing of plastics, the creation of electrical devices, lubricating flows, and the production of medical supplies. A theoretical analysis is conducted to examine the stagnation point flow of a 2nd-grade micropolar fluid into a porous material in the direction of a stretched surface under the magnetic field effect, which is stimulated by these applications. The stratification boundary conditions are imposed on the surface of the sheet. Generalized Fourier and Fick's laws with activation energy is also considered to discuss the heat and mass transportation. To obtain the dimensionless version of the flow modeled equations, an appropriate similarity variables are used. These transfer version of equations is solved numerically by the implement of the BVP4C technique on MATLAB. The graphical and numerical results are obtained for various emerging dimensionless parameters and discussed. It is noted that by the more accurate predictions of ε and M, the velocity sketch is decreased due to occurrence of resistance effect. Further, it is seen that larger estimation of micropolar parameter improves the angular velocity of the fluid.

The collective features of mixed convection and thermal radiation are the abundant consequences in the physiology of human organs such as the heart, liver, and brain. In medicine, science, engineering, and industrial processes, the investigations of mixed convection flow induced by stretching surfaces have a prominent application. These applications have been deliberated by distant investigators. Over a stretched sheet, Khan et al.[1] investigated the effects of non-linear thermal radiation, viscous dissipation, nonlinear convection, heat sink or source, and thermophoresis on hyperbolic tangent fluid flow with nanoparticles. In nonlinear mixed convection flow of the Newtonian fluid along a heat source or sink, double stratification, and nonlinear thermal radiation beneath the Riga plate, Hayat et al.[2] examined the mass-heat transmission. Ibrahim and Gizewu[3] discussed the transportation of heat and mass into the non-Newtonian tangent hyperbolic liquid with nanoparticles of non-linear mixed convection flow with Cattaneo–Christove model with the magnetic effect, activation energy past a non-uniform expandable sheet. Patil et al.[4] looked at the heat-mass transmission for a water-base fluid flowing in a non-linear mixed convection flow on a vertical cone. Alsaedi et al.[5] analyzed the heat-mass communication in the Eyring–Powell nanofluid non-linear mixed convection flow with the influence of magnetic effect, Joule heating, and viscous dissipation towards a stretched sheet. By Qasemian et al.[6], the hydraulic and thermal behaviour of a nanofluid flow inside a tube used in an automated transmission was examined. Fathellahi et al.[7] looked at how MHD affected the 2D squeezing flow of nanofluid between two evenly spaced sheets. Several studies of the non-linear mixed convection flow of different liquids can be found in Refs.[8–13].

[1]School of Energy and Power Engineering, Jiangsu University, Zhenjiang 212013, China. [2]Department of Mathematics, University of Sargodha, Sargodha 40100, Pakistan. [3]Department of Mathematics, Faculty of Science, University of Tabuk, P.O.Box 741, Tabuk 71491, Saudi Arabia. [4]Faculty of Engineering, Center of Research, Future University in Egypt, New Cairo 11835, Egypt. [5]Department of Mathematics, College of Science and Humanities in Al-Aflaj, Prince Sattam Bin Abdulaziz University, Al-Kharj, Saudi Arabia. [6]Mechanical Engineering Department, College of Engineering, King Khalid University, Abha 61421, Saudi Arabia. ✉email: zhentao.wang@ujs.edu.cn

Due to numerous applications of boundary layer flow in engineering and industrial processes like paper making, plastic sheet and film design, aerodynamic extrusion of plastic and rubber sheets, strengthening and dilution of copper wires, glass fibers, metallic surface cooling in a cooling bath, etc., which caused by a continuous stretched sheet has received significant attention over the past few years. Yurusoy and Pakdemirli[14] obtained the accurate solutions to the equations regulating the flow of a non-Newtonian fluid towards a stretched sheet. The visco-elastic fluid flow through a permeable media was described by Prasad et al.[15] as a result of the consequences of reaction rate on the transportation of chemically reactive species towards a stretched sheet. Riaz et al.[16] addressed the entropy generation impacts and irreversibility comparison flow of Cu-blood nanofluid flow under the applied magnetic field and viscous dissipation impacts through a curved channel. Nadeem et al.[17] investigated convection and diffusion analysis by mathematical assessment under the viscous dissipation into a noncircular duct. Elgazery and Hassan[18] investigated the influence of magnetic fields, permeable medium, thermal diffusivity, and variable viscosity for heat-mass transportation into a non-Newtonian liquid on a stretched surface. The heat-mass transmission of stagnation point of a non-Newtonian fluid flow under the effect of heterogeneous and homogeneous chemical processes via an expandable surface was established by Labropulu et al.[19]. Javed et al.[20] considered the flow of a non-Newtonian liquid with the Powell–Eyring model toward a stretching sheet. The few most current contributions in the stretching sheet may be indicated in the Refs.[21–24].

The transportation of heat and mass in the flow of non-Newtonian and Newtonian fluids towards a continuously moving sheet are very important in various industries, technological and engineering procedures such as control of the cooling rate, geophysics, crude oil purification, magnetic material processing, a metallic plate that is constantly cooling, discharge of plastic or rubbery sheets, spinning of fibers, glass blowing, continuous casting, taking filament or polymers out of a die, etc. The transmission of heat is a natural phenomenon that occurs due to the variation of temperature among bodies or within the same body. For two centuries, Fourier and Fick's diffusion laws of diffusion were the prevailing sources to depict the topography of the process of heat-mass communication, as a substitute for visualizing unique mass and thermal diffusion. This is agreeable with the statistic that changing relaxation times for the distribution of velocity should interrupt the temperature along with the concentration sketches. Liu[25] proved the heat-mass transmission in an MHD flow and created perfect solutions with heat production or absorption and a uniform magnetic field directed at a stretchy sheet. Sanjayanand and Khan[26] looked at the heat-mass transfer into the laminar flow of a second-grade fluid under the influence of elastic deformation and viscous dissipation through an exponentially stretched sheet. Qasim[27] scrutinized the collective consequences of heat-mass transmission in the Jaffrey fluid in the existence of a heat sink or source and surface temperature and surface mass convection with a stretching surface. In a MHD, 2-D, constant flow of an incompressible liquid in the existence of a porous material, thermal radiation, and a non-uniform magnetic effect past an extending vertical sheet, Rashidi et al.[28] considered mass and heat communication. In a rectangular chamber, heated spinning impediments caused convective heat transfer into the viscous fluid flow, which was studied by Nadeem et al.[29] statistically. Nadeem et al.[30] analyzed the generalized Fourier and Fick's law with double diffusion for the axisymmetric stagnation point flow of viscoelastic fluid having nanoparticles on the Riga plate. Ishtiq et al.[31] analysis of the hybrid nanofluid stagnation point flow towards a stretching/shrinking permeable sheet using the expanded Yavada-Ota and Xue model is based on the effects of MHD. In order to study how heat and mass are transferred into a second-grade fluid containing nanoparticles with the impact of the Cattaneo–Christov double diffusion and buoyancy forces, Nadeem et al.[32] looked at the variable thermal conductivity and variable viscosity. The importance of heat radiation for the time-dependent two-dimensional flow of third-grade fluid towards a permeable stretching sheet Riga plate was studied by Nadeem et al.[33]. Guedri et al.[34] discussed the impact of varying thermal conductivity, microrotation, thermal radiation, heat production, heat generation/absorption, and MHD for the flow of third-grade fluid towards an exponentially stretched sheet. Sandeep et al.[35] provided a comparative study of the heat-mass transmission of Oldroyd-B, Maxwell, and Jaffery fluids having nanoparticles under the effects of suction or injection, Brownian motion, thermophoresis, and transverse magnetic field towards a permeable expanding sheet. Qasim et al.[36] scrutinized the mass and heat transfer by using Burngiorno model in a thin film of nanofluid towards an unsteadily stretching sheet. For the flow of a hybrid nanofluid in a rotating system, Abdellahi et al.[37] quantitatively evaluated the mass and heat transfer. The heat and mass communication features of Newtonian and Non-Newtonian liquids were debated in distinct features by investigators for diverse physical parameters in the study[38–50].

In the present investigation the thermal and solutal transfer phenoneman is considered of the two-dimensional stagnation point flow of micropolar viscoelastic (second grade) fluid with the Cattaneo–Christov heat flux theory towards a stretched sheet. Further we consider to form novelty in the work activation energy, magnetic field, thermophoretic effect, and thermal radiation features. It has not been discussed the such type of issue so far. The numerical solution of the governing PDEs of the flow model after transformation into ODEs is achieved by using the BVP4C Matlab technique. Impacts of various parameters are studied with tables and diagrams across velocity, concentration, micropolar, and temperature distribution.

Mathematical expression

Here we consider a steady, 2D incompressible, stagnation point flow of a micropolar second grade fluid on a stretching surface with modified heat and mass flux. To scrutinize the aspects of mass-heat transportation the thermal radiation and activation energy effects are considered. Further, the thermal and stratification boundary conditions are implemented on the surface of the sheet. The physical model is displayed in the Fig. 1. The sheet is stretching with a velocity of $u = cx$ (here, c is the positive constant). The magnetic effect of strength B_0 is used along the y-direction. The temperature on the sheet is kept up at T_w and far away from the sheet is T_∞.

The model of 2nd-grade fluid, the Cauchy stress tensor is defined as[51],

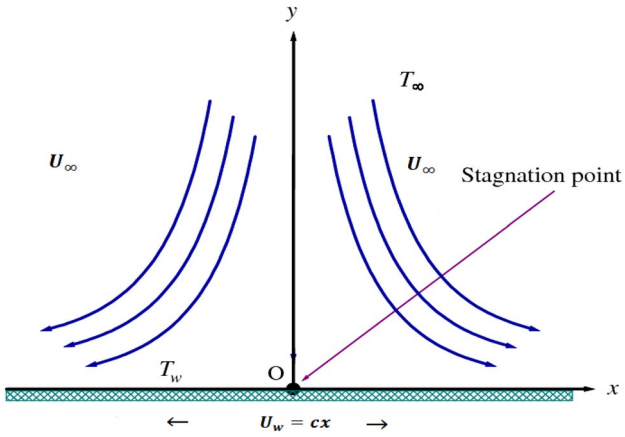

Figure 1. Flow mechanism.

$$T = -PI + \mu A_1 + \alpha_1 A_2 + \alpha_2 A_1^2, \tag{1}$$

where I is the identity tensor, μ is the dynamic viscosity, P is the pressure, $\alpha_i (i = 1,2)$ the material constants, A_1 and A_2 are two Rivlin–Ericksen tensors are

$$A_1 = (grad\, v) + (grad\, v)^T, \tag{2}$$

$$A_2 = \frac{dA_1}{dt} + A_1 (grad\, v) + (grad\, v)^T A_1. \tag{3}$$

Here, V is the velocity and $\frac{d}{dt}$ is the material time derivative. Keep in mind that when the fluid is in equilibrium and at rest locally, the Clausius–Duhem inequality is met, and the Helmboltz free energy is minimal.

$$\mu \geq 0, \alpha_1 \geq 0, \alpha_1 + \alpha_2 = 0. \tag{4}$$

It should be noticed that the constitutive equation of a fluid in the second grade simplifies to an equation for a viscous fluid when $\alpha_1 = \alpha_2 = 0$.

The momentum, continuity, and heat equations with some effects are as followed[52,53].

$$\frac{\partial u}{\partial x} + \frac{\partial v}{\partial y} = 0, \tag{5}$$

$$u\frac{\partial u}{\partial x} + v\frac{\partial u}{\partial y} = U_\infty \frac{dU_\infty}{dx} + \left(\frac{\mu + k}{\rho}\right)\frac{\partial^2 u}{\partial z^2} + \frac{k}{\rho}\frac{\partial N}{\partial z} + \frac{1}{\rho}\sigma B_0^2 (U_\infty - u) - \frac{\nu}{k_1}u + \frac{\alpha_1}{c_p \rho}\left[\frac{\partial}{\partial x}\left(u\frac{\partial^2 u}{\partial y^2}\right) + \frac{\partial u}{\partial y}\frac{\partial^2 v}{\partial v^2} + v\frac{\partial^3 u}{\partial y^3}\right], \tag{6}$$

$$u\frac{\partial N}{\partial x} + v\frac{\partial N}{\partial y} = \frac{\gamma}{j\rho}\frac{\partial^2 N}{\partial y^2} - \frac{k}{j\rho}\frac{\partial v}{\partial z} - \frac{2k}{j\rho}N, \tag{7}$$

$$\begin{aligned} &u\frac{\partial T}{\partial x} + v\frac{\partial T}{\partial y} + \lambda_E\left[\left(u\frac{\partial u}{\partial x} + v\frac{\partial u}{\partial y}\right)\frac{\partial T}{\partial x} + \left(v\frac{\partial v}{\partial y} + u\frac{\partial v}{\partial y}\right)\frac{\partial T}{\partial y} + 2uv\frac{\partial^2 T}{\partial x \partial y} + u^2\frac{\partial^2 T}{\partial x^2} + v^2\frac{\partial v}{\partial x}\right] \\ &= \alpha\frac{\partial^2 T}{\partial y^2} + \frac{\alpha_1}{\rho c_p}\left[\frac{\partial u}{\partial y}\left[\frac{\partial}{\partial y}\left(u\frac{\partial u}{\partial x} + v\frac{\partial u}{\partial y}\right)\right]\right] + \left(\frac{\mu + k}{\rho c_p}\right)\left(\frac{\partial u}{\partial y}\right)^2 - \frac{1}{\rho c_p}\frac{\partial q_r}{\partial y}, \end{aligned} \tag{8}$$

$$\begin{aligned} &u\frac{\partial C}{\partial x} + v\frac{\partial C}{\partial y} + \lambda_c\left[\left(u\frac{\partial u}{\partial x} + v\frac{\partial u}{\partial y}\right)\frac{\partial C}{\partial x} + \left(u\frac{\partial v}{\partial y} + v\frac{\partial v}{\partial y}\right)\frac{\partial C}{\partial y} + 2uv\frac{\partial^2 C}{\partial x \partial y} + u^2\frac{\partial^2 C}{\partial x^2} + v^2\frac{\partial^2 C}{\partial y^2}\right] \\ &= D_B\frac{\partial^2 C}{\partial y^2} - K_r{}^2\left(\frac{T}{T_\infty}\right)^m \exp\left(\left(\frac{-E_a}{\kappa T}\right)\right)(C - C_\infty) - \frac{\partial}{\partial y}(V_T C). \end{aligned} \tag{9}$$

The following boundary criteria apply in each case:

$$u = U_w = cx, v = 0, T = T_0 + \epsilon_1 x, C = C_w = C_0 + \epsilon_2 x, N = -n\frac{\partial u}{\partial y} \text{ at } y \to 0,$$

$$u \to U_\infty, T \to T_\infty = T_0 + \epsilon_3 x, C \to C_\infty = C_0 + \epsilon_4 x, N \to 0 \text{ at } y \to \infty. \tag{10}$$

The similarity transformations are as followed,

$$u = cxf^{'}, v = -\sqrt{c\nu}f, N = cxg, \theta = \frac{T - T_\infty}{T_w - T_\infty}, \phi = \frac{C - C_\infty}{C_w - C_\infty}, \eta = \sqrt{\frac{c}{\nu}}y. \tag{11}$$

Here, (u, v), are the components of velocity corresponding to (x, y).The symbols $U_e, \mu, k, \rho, N, c_p, \alpha_1, \sigma, B_0, g, \lambda_1, T, T_\infty, \lambda_2, \lambda_3, C, C_\infty, \lambda_4, \nu, k_1, \gamma, j, \lambda_E, \alpha, Q_0, q_r, \lambda_c, D_B, k_r, m, E_a, U_m, T_0, \epsilon_1, \epsilon_2, \epsilon_3, \epsilon_4, C_w, C_0$ and n are represented the free stream velocity, dynamic viscosity, vortex viscosity, density of the fluid, heat capacity, second grade fluid coefficient, electrical conductivity, magnetic field strength, gravity force, linear expansion coefficient, temperature, free stream temperature, non-linear mass expansion, linear mass expansion coefficient, fluid concentration, free stream concentration, non-linear mass expansion coefficient, kinematic viscosity, porous medium permeability, spin gradient, micro-inertia density, relaxation of heat flux, thermal conductivity, coefficient of heat sink/source4, thermal radiation coefficient, the relaxation of mass flux, Brownian motion coefficient, reaction rate coefficient, constant of fitted rate, coefficient of activation energy, wall velocity along x-axis, concentration, reference temperature, positive constants, concentration of fluid at wall, reference concentration and gyration parameter respectively.

The flow expressions in the non-dimensional form become,

$$(1+K)f''' + Kg' - f'^2 + ff'' - M^2(\in -f') + \in^2 + \beta\left[2f'f''' - f''^2 - ff^{(iv)}\right] - \varepsilon f' = 0, \tag{12}$$

$$\left(1 + \frac{K}{2}\right)g'' + fg'' - f'g - K(2g + f'') = 0, \tag{13}$$

$$\begin{aligned} &Prf\theta' - Pr(\theta + S)f' - Pr\delta_e\left[ff'\theta' + \theta''f^2 + (\theta + S)\left(f'^2 - ff''\right)\right] + Pr\beta f''\left[f'f'' - ff''\right] \\ &+ (1+K)Prf'^2 + \left[1 + R\left((1 + (\theta_w - 1)\theta)^3\right)\theta'\right]' = 0, \end{aligned} \tag{14}$$

$$\begin{aligned} &\phi'' - Sc(\phi + S^*)f' + Scf\phi' - Sc\delta_c\left[ff'\phi' + \phi''f^2 + (\phi + S^*)\left(f'^2 - ff''\right)\right] \\ &+ Sc\epsilon_5(1+\epsilon_6)^m e^{-\frac{E}{(1+\epsilon_6\theta)}}\phi - Sc\tau\left(\theta'\phi' + \theta''\phi\right) = 0. \end{aligned} \tag{15}$$

The comparable boundary conditions are as follows:

$$f = 0, f^{'} = 0, \theta = 1 - S, \phi = 1 - S^*, g = -nf''(0) \text{ as } \eta \to 0,$$

$$f' \to 1, \theta \to 0, \phi \to 0, g \to 0 \text{ at } \eta \to \infty, \tag{16}$$

where, $K = \frac{k}{\mu}$ (Micropolar fluid parameter), $M = \frac{\sigma_0 B_0^2}{\rho c}$ (Magnetic effect parameter), $\varepsilon = \frac{a}{c}$ (Velocity ratio parameter), $\beta = \frac{\alpha_1 c}{\nu}$ (Second grade fluid parameter), $\in = \frac{\nu}{k_0 c}$ (Porous medium parameter), $L_e = \frac{k}{\rho c_p D_B}$ (Lewis number), $S_c = \frac{\nu}{D_B}$ (Simdth number), $\delta_c = \lambda_c c$ (Concentration relaxation time parameter), $\epsilon_5 = \frac{k_r^2}{c}$ (Parameter of chemical reaction), $\epsilon_6 = \frac{T_w - T_\infty}{T_\infty}$ (Parameter of temperature difference), $E = \frac{E_a}{\kappa T_\infty}$ (Activation energy parameter), $S = \frac{\epsilon_3}{\epsilon_1}$ (Thermal stratification parameter), $S^* = \frac{\epsilon_4}{\epsilon_2}$ (Concentration stratification parameter), $Pr = \frac{\rho c_p \nu}{k}$ (Prandtl number), $R = \frac{16\sigma^* T_\infty^3}{3kk^*}$ (Radiation parameter), $\theta_w = \frac{T_w}{T_\infty}$ (Temperature ratio parameter), $\delta_e = \lambda_E c$ (thermal relaxation time parameter).

Skin friction. From an engineering perspective, skin friction is very important physical quantities, which is stated by,

$$C_{fx} = \frac{\tau_w}{\frac{1}{2}\rho {u_w}^2}, \tag{17}$$

$$\tau_w = \left[\frac{\alpha_1}{\rho}\left(u\frac{\partial^2 u}{\partial y^2} - 2\frac{\partial u}{\partial x}\frac{\partial v}{\partial y} + u\frac{\partial^2 u}{\partial x \partial y}\right) + \left(\frac{\mu + k}{\rho}\right)\frac{\partial u}{\partial y} + kN_1\right]_{|y=0}. \tag{18}$$

In the dimensionless form,

$$C_{fx_{|\eta=0}} = \left[\beta\left(3f'(0)f''(0) - ff''(0)\right) + (1+K)f''(0)\right]\left(\frac{R_{ex}}{2}\right)^{-\frac{1}{2}}, \tag{19}$$

where $R_{ex} = \frac{xu_w}{\nu}$ is the Reynolds number.

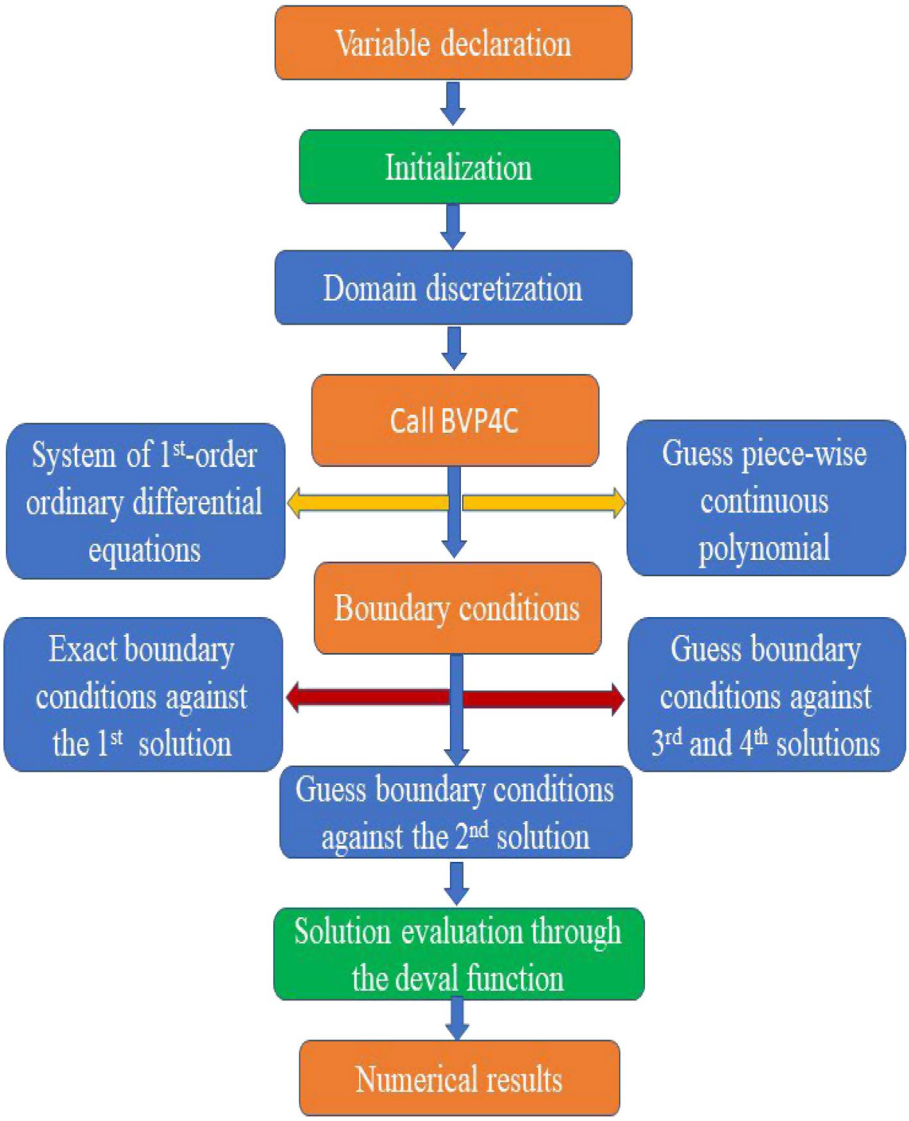

Figure 2. Numerical scheme.

Methodology

In this section, the two-dimensional viscoelastic fluid flow with modified heat and mass flux toward a stretching sheet is inspected numerically by using the BVP4C MATLAB approach. To used BVP4C first we convert the nonlinear ordinary differential equations into form system of first order differential equations. For this conversion we consider the momentum, micropolar, temperature, and concentration Eqs. (12)–(15) with boundary equation conditions (16) and convert them into the new variables. Moreover, numerical scheme is given in Fig. 2. In this instance, the new variables are introduced as follows:

$$\begin{array}{l} f = y_1, f''' = y_4, f' = y_2, f'' = y_3, f'''' = yy_1 \\ g = y_5, g' = y_6, g'' = yy_2 \\ \theta = y_7, \theta' = y_8, \theta'' = (y_8)\prime \\ \phi = y_9, \phi' = y_{10}, \phi'' = yy_4 \end{array}, \tag{23}$$

$$yy_1 = \frac{1}{\beta}\left\{Ky_6 - \beta\left(y_3^2 - 2y_2y_4\right) - (1+K)y_4 - y_2^2 + y_1y_3 - M^2\left(\epsilon - y_2\right) + \epsilon^2 - \varepsilon y_2\right\}, \tag{24}$$

$$yy_2 = \frac{1}{\left(1 + \frac{K}{2}y_1\right)}\left\{y_1y_6 + K\left(2y_5 + y_3\right)\right\}, \tag{25}$$

$$\left(y_8\right)' + Pr\left(\left(1 + R\left((1 + (\theta_w - 1)\theta)^3\right)\right)y_8\right)' = \frac{1}{\left(1 + PrS_c y_1^2\right)}\left\{Pr\delta_e\left[y_1 y_2 y_8 + \left(y_7 + S\right)\right.\right.$$
$$\left.\left.\left(y_2^2 - y y_3\right)\right] - Pr y_1 y_8\right\} - Pr\beta y_3\left(y_2 y_3 - y_1 y_3\right) - (1 + K)Pr y_2^2, \tag{26}$$

$$y y_4 = \frac{1}{\left(1 + Sc y_1^2 - Pr\delta_c y_1^2\right)}\left\{Sc y_1 y_2 y_{10} + PrSc\left(y_1 y_2 y_{10} + \left(y_9 + S^*\right)\left(y_2^2 - y_1 y_3\right)\right.\right.$$
$$\left.\left. - Sc\epsilon_5(1 + \epsilon_6)^m e^{-\frac{E}{(1+\epsilon_6 y_7)}y_9} + Sc\tau\left(y_8 y_{10} + y y_3 y_9\right)\right)\right\}. \tag{27}$$

Numerical results

In this section the details analysis of numerical data is pretested in the Table 1 for several physical parameters, such as K, M, β_t, and ε along the skin friction. According to Table 1, it is noted that greater estimation of K and M leads to higher $f\prime(0)$ values. Table 1 illustrates the impact of β_t on the $f\prime(0)$. It is observed that greater values of β_t and ε leads to higher estimates of skin friction $f\prime(0)$. The comparison between the current findings of the second-grade fluid parameter influence on skin friction and Rafiq et al.[54] is shown in Table 2. The results of the present study shows great harmony with previous data. This comparison gives us confidence in the results.

Graphical analysis

The following illustrations are created in order to examine variation of various parameters on the linear and angular velocity, temperature, and concentration profiles. Different estimations are given for the $\beta, M, \varepsilon, K, \delta_e, Pr, R, \theta_w, S, Sc, E$, and S^* to see the effects of them on heat transfer and fluid flow.

Linear and angular velocity profile analysis. The effect of the viscoelastic fluid parameter (β) on the velocity of the second-grade micropolar fluid in the boundary layer is revealed in Fig. 3a. The velocity of fluid rises when the viscoelastic fluid parameter is given greater values. Physically, by enhancing the estimations parameter of the viscoelastic fluid, the viscosity of fluid diminishes, therefore, that creates the momentum boundary layer dense. The velocity sketch effect on the magnetic field parameter (M) is perceived in Fig. 3b. It is noticed that the fluid velocity declines as the magnetic field parameter (M) gets stronger estimated. Physically, upsurge with the magnetic field parameter (M), upshots in a dominant decrease inside the corresponding velocity. Physically, the magnetic effect makes a retarding body force that is renowned as Lorentz force that creates

K	M	β_t	ε	C_{f_x}
0.1				1.4423
0.2				1.7560
0.3				1.6374
	0.1			1.5337
	0.2			1.7613
	0.3			2.0920
		0.1		1.8363
		0.2		1.8774
		0.3		1.9374
			0.1	15.7372
			0.2	16.3725
			0.3	17.0864

Table 1. The estimations of the skin friction coefficient for the stronger estimations of K, M, β_t, and ε.

	Present results	Rafiq et al.[54]
β	$f''(0)$	$f''(0)$
0.0	− 2.2537	− 2.24676880475314
0.2	− 4.1226	− 4.09820479923631
0.5	− 6.9593	− 6.93689203353080
0.7	− 9.4330	− 9.40436723010559
1.0	− 13.8760	− 13.8596936496045
2.0	− 59.8754	− 59.2327101256866

Table 2. Numerical results of skin friction compared with present results.

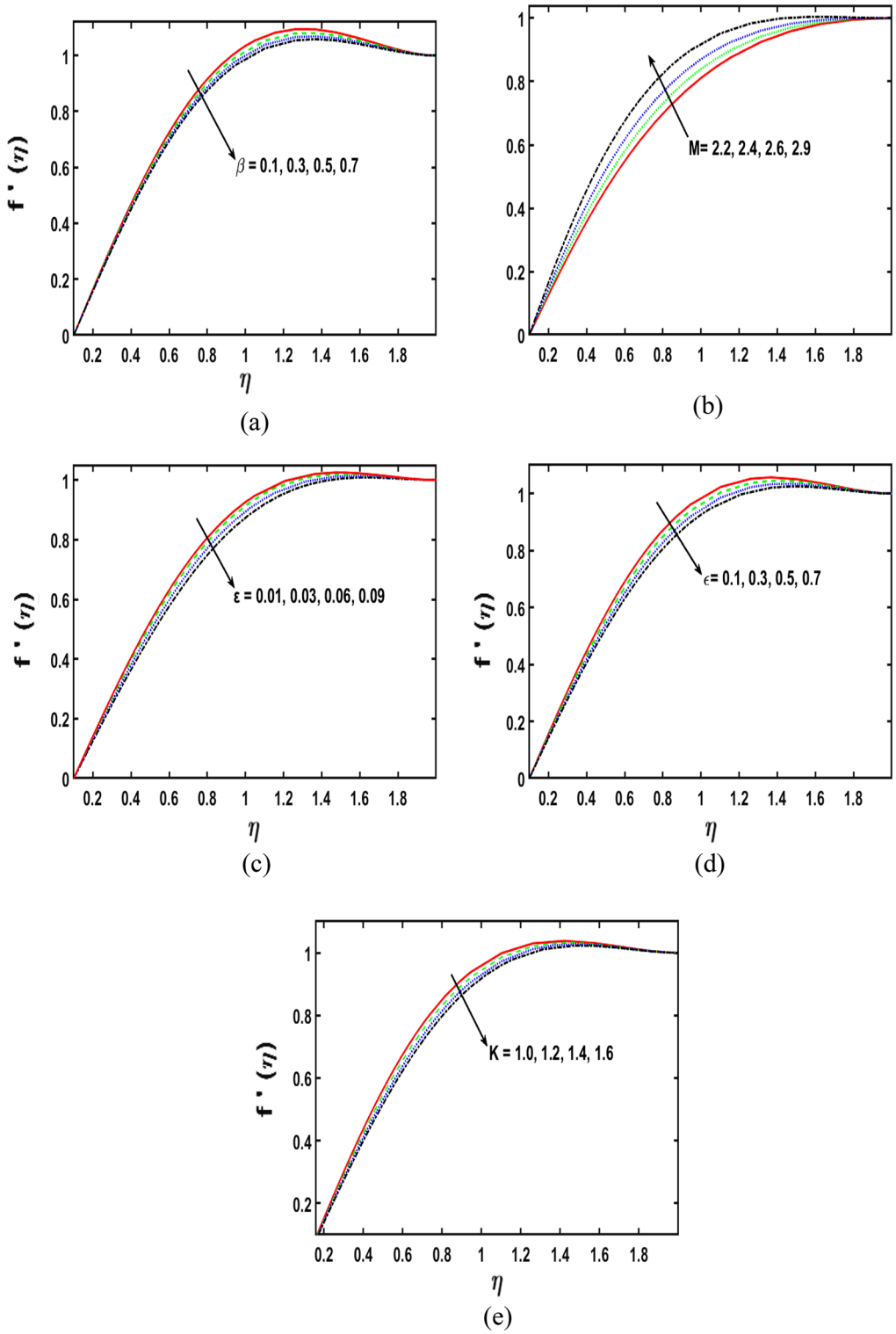

Figure 3. (**a–e**) Deviation in $\beta, M, \varepsilon, \epsilon$, and K along the velocity profiles.

more resistance to the velocity of the fluid. Moreover, this force produces more resistance to the mass transportation phenomenon. Figure 3c illustrates the influence of the parameter of stagnation point flow (ε) on the fluid velocity draft. By the stronger values of (ε), the velocity sketch decreases. Physically, the velocity distribution and the corresponding boundary layer thickness are boosted, for stronger estimations of ε, therefore, the velocity sketch reduces. Figure 3d displays the performance of porous medium parameter (ϵ) on the velocity sketch. It is distinguished that the velocity profile reduces for aggregating the variations of porous medium parameter (ϵ).

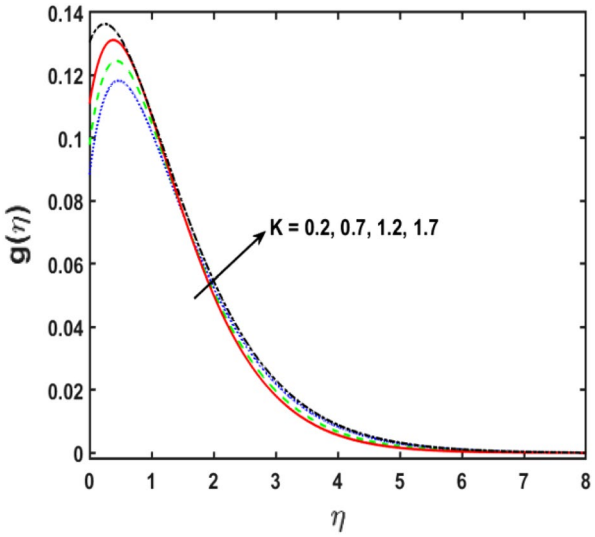

Figure 4. Deviation in K for micropolar profile.

Figure 3e illustrates the impact of the micropolar fluid parameter (K) on the velocity sketch. It is perceived that for K, the velocity sketch boosts as the upsurge in the variations of the estimations of K. Therefore, It is obvious that the boundary layer thickness augmented for K. The relationship between the angular velocity and the micropolar fluid parameter is shown in the Fig. 4. The figure illustrates that when the estimates of the micropolar fluid parameter K improves, the angular velocity also increases.

Temperature profile analysis. The consequence of viscoelastic fluid parameter β on the temperature sketch in Fig. 5a. It is found that with an upsurge in the second-grade fluid parameter, the temperature profile grows, consequently, the corresponding thermal boundary layer rises. From Fig. 5b, it is noted that the temperature field declines for the stronger variations of the thermal relaxation parameter δ_e. Physically, the parameter of the time relaxation gives the corresponding condition for temperature exchange and decays the boundary layer thickness. Consequently, the liquid viscosity will be a little increased. The behavior of $\theta(\eta)$ for the improving estimations of Pr is shown in the Fig. 5c. The thick dispersion frequency to the thermal dispersion frequency is therefore defined as the Pr. The aftereffects of the non-linear thermal radiation parameter (R) on the $\theta(\eta)$ are observed in Fig. 5d. It is displayed that the $\theta(\eta)$ enhances owing to the improving estimations of thermal radiation parameter. The increasing values of the thermal radiation parameter are what determine the thickness of the thermal boundary layer. Figure 5e depicts how the temperature ratio parameter affects the temperature sketch. It is depicted that the temperature profile increases due to the stringer estimations of temperature ratio parameter θ_w. Figure 5f displays the variation of temperature sketch to see the effect of thermal stratification parameter S on temperature profile. The temperature sketch decreases for greater estimates of the thermal stratification parameter S. Physically, when the estimates of S are improved, the thermal boundary layer thickness decreases.

Concentration profile analysis. Figure 6a demonstrates the upshot of the concentration relaxation parameter δ_c on the $\phi(\eta)$ draft. It is clear that by enhancing the concentration relaxation parameter δ_c, the concentration profile diminishes. Physically, by boosting the estimations of δ_c, the concentration boundary layer acquires thinner. Figure 6b describes the influence of the E (activation energy parameter) on the concentration sketch. By improving the parameter of the activation energy parameter, the increment is observed in the concentration sketch. Physically, the Arrhenius function diminishes if the activation energy parameter E upsurge. Figure 6c depicts the impact of Schmidt number Sc on the concentration outline. Through raising the estimates of Schmidt number Sc, a decrement is seen in the concentration sketch. Since the Schmidt number is defined as the proportion of momentum to mass diffusivity. Figure 6d explains the deviation of concentration sketch under the impact of concentration stratification parameter S^*. It is seen that, by growing the parameter of the concentration stratification parameter S^* the concentration sketch reduces.

Concluding remarks

In the present research article, the heat and mass transport analysis of 2D stagnation point flow of micropolar second-order fluid past a stretchable sheet with Cattaneo–Cristove heat flux theory and stratification effect are examined numerically. Some useful outcomes of this work are given as,

- The enhancement in the velocity sketch is noticed for the stronger estimates of the 2nd-grade fluid parameter (β).
- With stronger M and ε estimates, declines in the velocity sketch.
- The velocity profile is improved by the increasing the estimation of K.

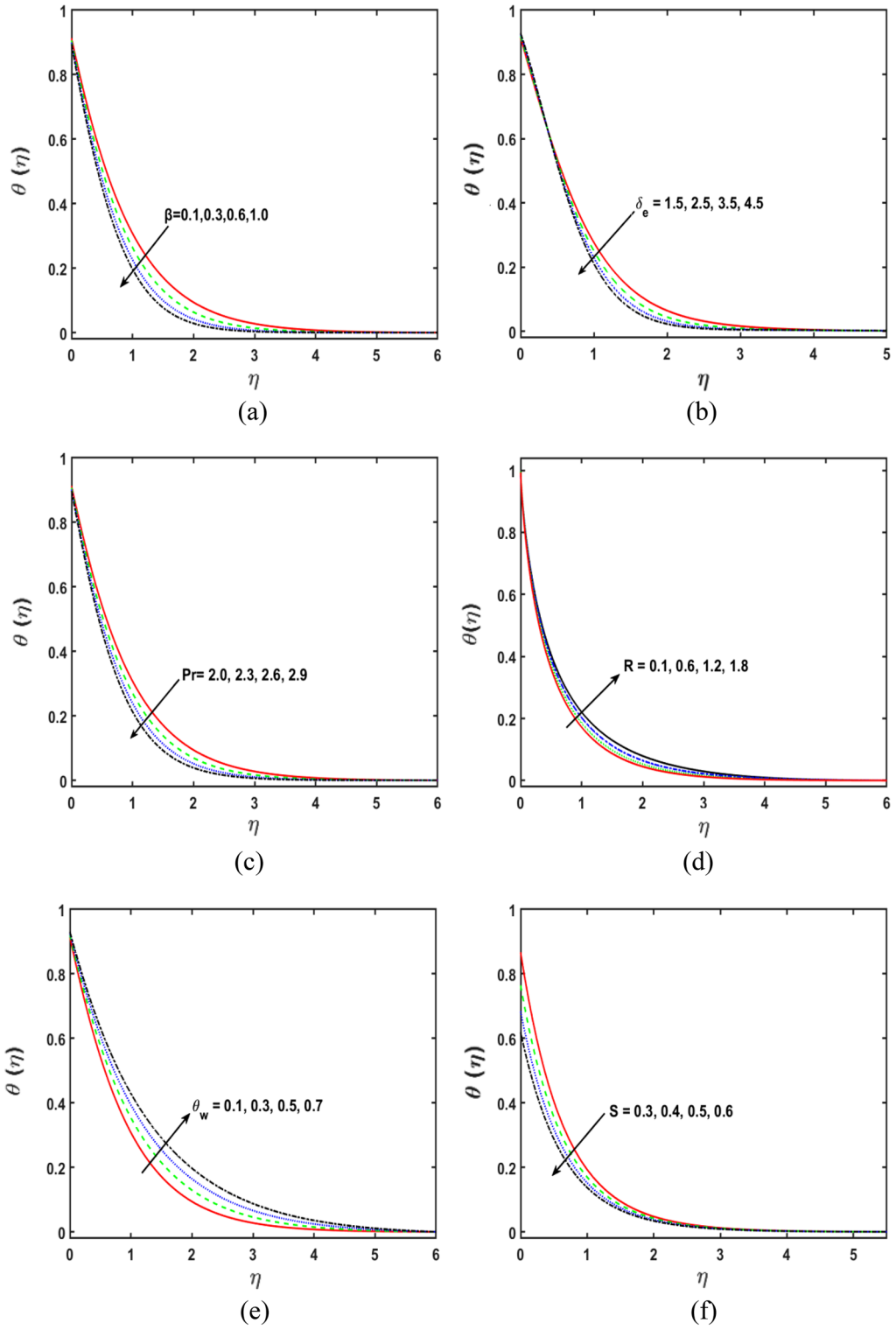

Figure 5. (**a–g**) Deviation in $\beta, \delta_e, Pr, R, \theta_w, and\ S$ along temperature profile.

- The angular velocity of the fluid upsurges due to the stronger values of K.
- The stronger estimations of β and δ_e leads to the decay of the temperature sketch.
- The temperature profile diminishes for Pr and improves for stronger estimation of R.
- As higher values of thermal stratification parameter the temperature profile increases.
- The skin friction coefficient shows an increasing behavior for improving values of K, β, M, and ϵ.
- For larger values of S^* declines the concentration profile.

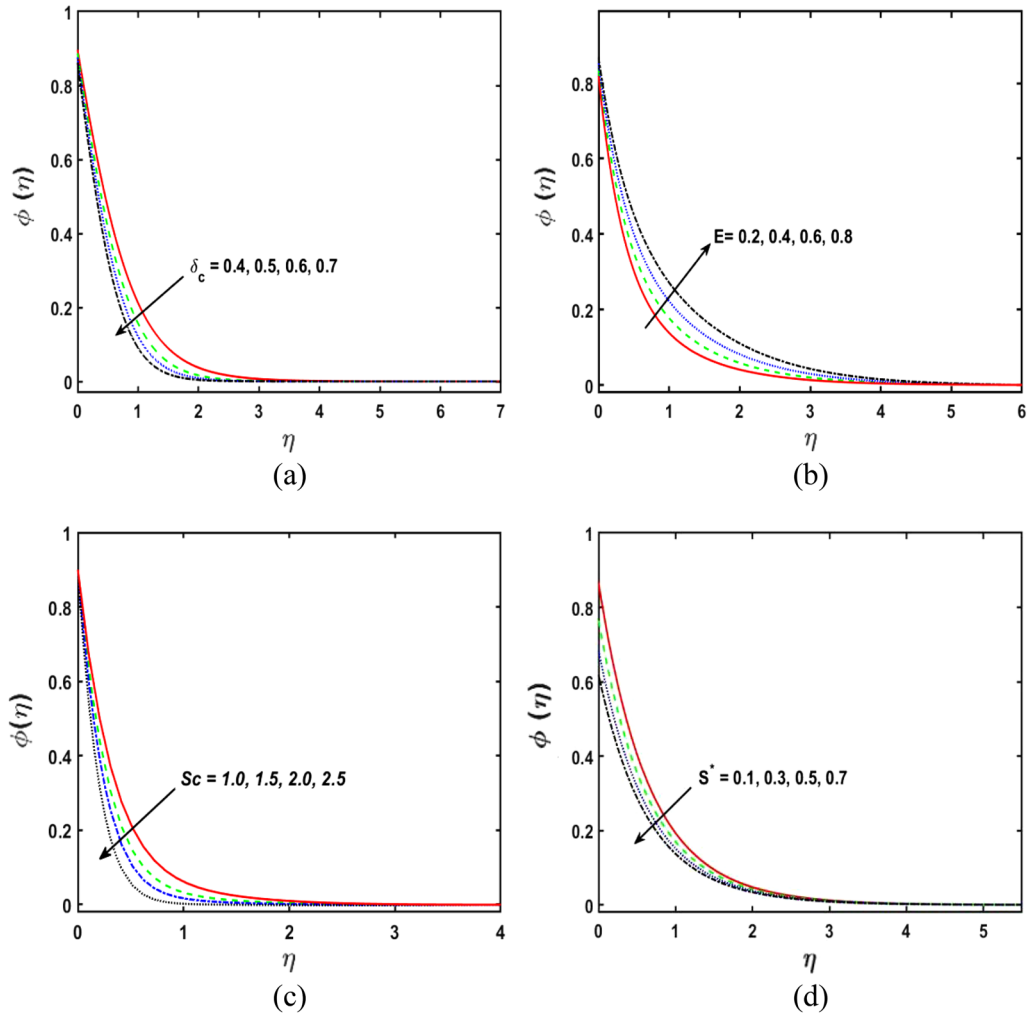

Figure 6. (**a,d**) Deviation in δ_c, E, Sc, and S^* vs concentration profile.

Data availability

The data that support the findings of this study are available from the corresponding author upon reasonable request.

Received: 8 February 2023; Accepted: 7 June 2023
Published online: 11 June 2023

References

1. Khan, M. I. *et al.* Entropy generation optimization and activation energy in nonlinear mixed convection flow of a tangent hyperbolic nanofluid. *Eur. Phys. J. Plus* **133**(8), 1–20 (2018).
2. Hayat, T., Ullah, I., Alsaedi, A. & Ahamad, B. Simultaneous effects of nonlinear mixed convection and radiative flow due to Riga-plate with double stratification. *J. Heat Transf.* **140**, 10 (2018).
3. Ibrahim, W. & Gizewu, T. Nonlinear mixed convection flow of a tangent hyperbolic fluid with activation energy. *Heat Transf.* **49**(5), 2427–2448 (2020).
4. Patil, P. M., Shashikant, A. & Hiremath, P. S. Diffusion of liquid hydrogen and oxygen in nonlinear mixed convection nanofluid flow over vertical cone. *Int. J. Hydrogen Energy* **44**(31), 17061–17071 (2019).
5. Alsaedi, A., Hayat, T., Qayyum, S. & Yaqoob, R. Eyring–Powell nanofluid flow with nonlinear mixed convection: Entropy generation minimization. *Comput. Methods Prog. Biomed.* **186**, 105183 (2020).
6. Qasemian, A., Moradi, F., Karamati, A., Keshavarz, A. & Shakeri, A. Hydraulic and thermal analysis of automatic transmission fluid in the presence of nano-particles and twisted tape: An experimental and numerical study. *J. Central South Univ.* **28**(11), 3404–3417 (2021).
7. Fathollahi, R., Alizadeh, A. A., Kamaribidkorpeh, P., Abed, A. M. & Pasha, P. Analyzing the effect of radiation on the unsteady 2D MHD Al2O3–water flow through parallel squeezing sheets by AGM and HPM. *Alex. Eng. J.* **69**, 207–219 (2023).
8. Irfan, M., Khan, W. A., Khan, M. & Gulzar, M. M. Influence of Arrhenius activation energy in chemically reactive radiative flow of 3D Carreau nanofluid with nonlinear mixed convection. *J. Phys. Chem. Solids* **125**, 141–152 (2019).
9. Iranmanesh, R. *et al.* Introducing a linear empirical correlation for predicting the mass heat capacity of biomaterials. *Molecules* **27**(19), 6540 (2022).
10. Khan, M. I. *et al.* Entropy generation in radiative motion of tangent hyperbolic nanofluid in presence of activation energy and nonlinear mixed convection. *Phys. Lett. A* **382**(31), 2017–2026 (2018).

11. Hayat, T., Haider, F. & Alsaedi, A. Darcy–Forchheimer flow with nonlinear mixed convection. *Appl. Math. Mech.* **41**(11), 1685–1696 (2020).
12. Waqas, M., Ullah, I., Hayat, T. & Alsaedi, A. Nonlinear mixed convection impact on radiated flow of nanomaterials subject to convective conditions. *Arab. J. Sci. Eng.* **46**(3), 2349–2359 (2021).
13. Yürüsoy, M. & Pakdemirli, M. Exact solutions of boundary layer equations of a special non-Newtonian fluid over a stretching sheet. *Mech. Res. Commun.* **26**(2), 171–175 (1999).
14. Prasad, K. V., Abel, S. & Datti, P. S. Diffusion of chemically reactive species of a non-Newtonian fluid immersed in a porous medium over a stretching sheet. *Int. J. Non-Linear Mech.* **38**(5), 651–657 (2003).
15. Riaz, A. *et al.* Insight into the cilia motion of electrically conducting Cu–blood nanofluid through a uniform curved channel when entropy generation is significant. *Alex. Eng. J.* **61**(12), 10613–10630 (2022).
16. Nadeem, S. *et al.* Mathematical assessment of convection and diffusion analysis for a non-circular duct flow with viscous dissipation: Application of physiology. *Symmetry* **14**(8), 1536 (2022).
17. Elgazery, N. S. & Hassan, M. A. The effects of variable fluid properties and magnetic field on the flow of non-Newtonian fluid film on an unsteady stretching sheet through a porous medium. *Commun. Numer. Methods Eng.* **24**(12), 2113–2129 (2008).
18. Labropulu, F., Li, D. & Pop, I. Non-orthogonal stagnation-point flow towards a stretching surface in a non-Newtonian fluid with heat transfer. *Int. J. Therm. Sci.* **49**(6), 1042–1050 (2010).
19. Javed, T., Ali, N., Abbas, Z. & Sajid, M. Flow of an Eyring–Powell non-Newtonian fluid over a stretching sheet. *Chem. Eng. Commun.* **200**(3), 327–336 (2013).
20. Khan, Y. & Latifizadeh, H. Application of new optimal homotopy perturbation and Adomian decomposition methods to the MHD non-Newtonian fluid flow over a stretching sheet. *Int. J. Numer. Methods Heat Fluid Flow* **24**, 124 (2014).
21. Ibrahim, S. M., Kumar, P. V. & Makinde, O. D. Chemical reaction and radiation effects on non-Newtonian fluid flow over a stretching sheet with non-uniform thickness and heat source. *Defect Diffus. Forum* **387**, 319–331 (2018).
22. Mishra, S. R., Shamshuddin, M. D., Beg, O. A. & Kadir, A. Adomain computation of radiative–convective bi-directional stretching flow of a magnetic non-Newtonian fluid in porous media with homogeneous–heterogeneous reactions. *Int. J. Mod. Phys. B* **34**(18), 2050165 (2020).
23. Sarada, K., Gowda, R. J. P., Sarris, I. E., Kumar, R. N. & Prasannakumara, B. C. Effect of magnetohydrodynamics on heat transfer behaviour of a non-Newtonian fluid flow over a stretching sheet under local thermal non-equilibrium condition. *Fluids* **6**(8), 264 (2021).
24. Abbas, W. & Megahed, A. M. Numerical solution for chemical reaction and viscous dissipation phenomena on non-Newtonian MHD fluid flow and heat mass transfer due to a nonuniform stretching sheet with thermal radiation. *Int. J. Mod. Phys. C* **32**(09), 1–20 (2021).
25. Liu, I. C. A note on heat and mass transfer for a hydromagnetic flow over a stretching sheet. *Int. Commun. Heat Mass Transf.* **32**(8), 1075–1084 (2005).
26. Sanjayanand, E. & Khan, S. K. On heat and mass transfer in a viscoelastic boundary layer flow over an exponentially stretching sheet. *Int. J. Therm. Sci.* **45**(8), 819–828 (2006).
27. Qasim, M. Heat and mass transfer in a Jeffrey fluid over a stretching sheet with heat source/sink. *Alex. Eng. J.* **52**(4), 571–575 (2013).
28. Rashidi, M. M., Rostami, B., Freidoonimehr, N. & Abbasbandy, S. Free convective heat and mass transfer for MHD fluid flow over a permeable vertical stretching sheet in the presence of the radiation and buoyancy effects. *Ain Shams Eng. J.* **5**(3), 901–912 (2014).
29. Nadeem, S., Haider, J. A., Akhtar, S. & Ali, S. Numerical simulations of convective heat transfer of a viscous fluid inside a rectangular cavity with heated rotating obstacles. *Int. J. Mod. Phys. B* **36**(28), 2250200 (2022).
30. Nadeem, S., Ishtiaq, B., Almutairi, S. & Ghazwani, H. A. Impact of Cattaneo–Christov double diffusion on 3d stagnation point axisymmetric flow of second-grade nanofluid towards a riga plate. *Int. J. Mod. Phys. B* **36**(29), 2250205 (2022).
31. Ishtiaq, B., Zidan, A. M., Nadeem, S. & Alaoui, M. K. Scrutinization of MHD stagnation point flow in hybrid nanofluid based on the extended version of Yamada-Ota and Xue models. *Ain Shams Eng. J.* **14**(3), 101905 (2023).
32. Nadeem, S., Tumreen, M., Ishtiaq, B., Abbas, N. & Shatanawi, W. Second-grade nanofluid flow above a vertical slandering Riga surface with double diffusion model. *Int. J. Mod. Phys. B* **36**(32), 2250237 (2022).
33. Nadeem, S., Ishtiaq, B. & Abbas, N. Impact of thermal radiation on two-dimensional unsteady third-grade fluid flow over a permeable stretching Riga plate. *Int. J. Mod. Phys. B* **37**(01), 2350009 (2023).
34. Guedri, K. *et al.* Insight into the heat transfer of third-grade micropolar fluid over an exponentially stretched surface. *Sci. Rep.* **12**(1), 15577 (2022).
35. Sandeep, N., Kumar, B. R. & Kumar, M. J. A comparative study of convective heat and mass transfer in non-Newtonian nanofluid flow past a permeable stretching sheet. *J. Mol. Liq.* **212**, 585–591 (2015).
36. Qasim, M., Khan, Z. H., Lopez, R. J. & Khan, W. A. Heat and mass transfer in nanofluid thin film over an unsteady stretching sheet using Buongiorno's model. *Eur. Phys. J. Plus* **131**(1), 1–11 (2016).
37. Abdollahi, S. A., Alizadeh, A. A., Zarinfar, M. & Pasha, P. Investigating heat transfer and fluid flow betwixt parallel surfaces under the influence of hybrid nanofluid suction and injection with numerical analytical technique. *Alex. Eng. J.* **70**, 423–439 (2023).
38. Alizadeh, A. A. *et al.* Numerical investigation of the effect of the turbulator geometry (disturber) on heat transfer in a channel with a square section. *Alex. Eng. J.* **69**, 383–402 (2023).
39. Fatehinasab, R., Shafiee, H., Afshari, M. & Pasha, P. Hybrid surveying of radiation and magnetic impacts on Maxwell fluid with MWCNT nanotube influence of two wire loops. *ZAMM J. Appl. Math. Mech.* **103**(1), e202200186 (2023).
40. Sreedevi, P., Reddy, P. S. & Chamkha, A. Heat and mass transfer analysis of unsteady hybrid nanofluid flow over a stretching sheet with thermal radiation. *SN Appl. Sci.* **2**(7), 1–15 (2020).
41. Venkata Ramudu, A. C., Anantha Kumar, K., Sugunamma, V. & Sandeep, N. Heat and mass transfer in MHD Casson nanofluid flow past a stretching sheet with thermophoresis and Brownian motion. *Heat Transf.* **49**(8), 5020–5037 (2020).
42. Srinivasulu, T. & Goud, B. S. Effect of inclined magnetic field on flow, heat and mass transfer of Williamson nanofluid over a stretching sheet. *Case Stud. Therm. Eng.* **23**, 100819 (2021).
43. Sudarsana Reddy, P. & Sreedevi, P. Impact of chemical reaction and double stratification on heat and mass transfer characteristics of nanofluid flow over porous stretching sheet with thermal radiation. *Int. J. Ambient Energy* **43**(1), 1626–1636 (2022).
44. Nadeem, S., Ahmad, S., Issakhov, A. & Alarifi, I. M. MHD stagnation point flow of nanofluid with SWCNT and MWCNT over a stretching surface driven by Arrhenius kinetics. *Appl. Math. A J. Chin. Univ.* **37**(3), 366–382 (2022).
45. Muhammad, N., Nadeem, S. & Zaman, F. D. Transmission of thermal energy in a ferromagnetic nanofluid flow. *Int. J. Mod. Phys. B* **36**(32), 2250236 (2022).
46. Shahzad, M. H. *et al.* Sensitivity analysis for Rabinowitsch fluid flow based on permeable artery constricted with multiple stenosis of various shapes. *Biomass Convers. Bioref.* **1**, 1–11 (2022).
47. Nadeem, S., Akhtar, S., Saleem, A., Almutairi, S., Ghazwani, H. A. & Eldin, S. M. *Numerical Analysis for the Hemodynamics Mechanism of a Curved Artery Having Multiple Stenosis* (2022).
48. Ishtiaq, B., Nadeem, S. & Abbas, N. Theoretical study of two-dimensional unsteady Maxwell fluid flow over a vertical Riga plate under radiation effects. *Sci. Iran.* **29**(6), 3072–3083 (2022).
49. Haider, J. A., Asghar, S. & Nadeem, S. Travelling wave solutions of the third-order KdV equation using Jacobi elliptic function method. *Int. J. Mod. Phys. B* **1**, 2350117 (2022).

50. Nadeem, S., Tumreen, M., Ishtiaq, B. & Abbas, N. Three-dimensional second-grade nanofluid flow with MHD effects through a slandering stretching sheet: A numerical solution. *Waves Random Complex Media* **1**, 1–19 (2022).
51. Abbas, Z., Hayat, T., Sajid, M. & Asghar, S. Unsteady flow of a second grade fluid film over an unsteady stretching sheet. *Math. Comput. Model.* **48**(3–4), 518–526 (2008).
52. Abbas Khan, A. *et al.* Flow investigation of second grade micropolar nanofluid with porous medium over an exponentially stretching sheet. *J. Appl. Biomater. Funct. Mater.* **20**, 22808000221089784 (2022).
53. Nabwey, H. A. *et al.* Computational analysis of the magnetized second grade fluid flow using modified Fourier and Fick's Law towards an exponentially stretching sheet. *Mathematics* **10**(24), 4737 (2022).
54. Rafiq, M. *et al.* Analytical solution for the flow of second grade fluid over a stretching sheet. *AIP Adv.* **9**(5), 055313 (2019).

Acknowledgements
The authors extend their appreciation to the Deanship of Scientific Research at King Khalid University for funding this work through large group Research Project under Grant Number RGP2/153/44.

Author contributions
M.N.K.: Conceptualization, Methodology, A.A.K.: Software, Writing-Original Draft Preparation, Visualization, Validation, Z.W.: Supervision and evaluation, Method validation and coding, H.F.A.: Writing: review & editing, S.M.E.: Reviewing and Editing, F.M.A.: Formal analysis, Data correction, I.E.E.: Modelling of the problem.

Funding
The funding was provided by Sayed M Eldin.

Competing interests
The authors declare no competing interests.

Additional information
Correspondence and requests for materials should be addressed to Z.W.

Reprints and permissions information is available at www.nature.com/reprints.

Publisher's note Springer Nature remains neutral with regard to jurisdictional claims in published maps and institutional affiliations.